Mini Review

Band edge exciton in CdSe and other II-VI and III-V compound semiconductor nanocrystals -revisited

Pete C Sercel, and Alexander L. Efros

Nano Lett., **Just Accepted Manuscript** • DOI: 10.1021/acs.nanolett.8b01980 • Publication Date (Web): 21 Jun 2018

Band edge exciton in CdSe and other II-VI and III-V compound semiconductor nanocrystals – Revisited

Peter C. Sercel*,† and Alexander L. Efros*,‡

†*T. J. Watson Laboratory of Applied Physics, California Institute of Technology, Pasadena, California 91125, USA*

‡*Naval Research Laboratory, Washington DC 20375, USA*

E-mail: psercel@caltech.edu; efros@nrl.navy.mil

Abstract

In this letter we summarize major corrections to the dark/bright exciton theory [Al. L. Efros et al, Phys. Rev B **54**, 4843-4856 (1996)] which should be used for quantitative description of the band edge exciton in II-VI and III-V compound quantum dot nanocrystals (NCs). The theory previously did not take into account the long-range exchange interaction, resulting in the underestimation of the splitting between the upper bright and lower dark or quasi-dark exciton, as reported by several experimental groups. Another type of correction originates from the closeness in energy of the ground, $1S_{3/2}$, and the first excited, $1P_{3/2}$, hole levels in a spherical NC resulting in significant energetic overlap of the levels from the $1S_{3/2}1S_e$ and $1P_{3/2}1S_e$ exciton manifolds connected with the ground $1S_e$ electron level. The thermal occupation of the optically forbidden $1P_{3/2}1S_e$ exciton levels changes the radiative decay time of the NCs both at helium and at room temperatures. We demonstrate the role of both effects in CdSe NCs, and compare our predictions with available experimental data.

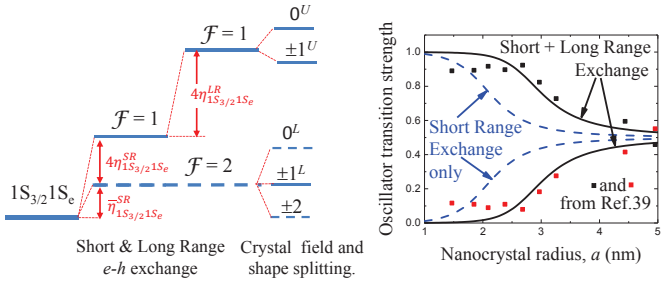

KEYWORDS: Exciton fine structure, nanocrystals, short- and long- range electron-hole exchange interaction, hole level structure.

Introduction

In practically all bulk semiconductors and all existing semiconductor hetero-structures the ground exciton state is an optically passive "dark" exciton. The direct optical excitation of this state by a single photon or its direct photon emission is forbidden due to the parallel alignment of the electron and hole spin states caused by the ferromagnetic character of the electron-hole exchange interaction. Only exciton states with anti-parallel alignment of the electron and hole spins ("bright" exciton states) can be excited directly by a photon and directly emit a photon. The only known exception to this rule was reported just recently,[1] where it was proposed that 10–15 nm size lead-halide perovskite nanocrystals (NCs) have a bright ground exciton state.

In bulk semiconductors,[2] epitaxial quantum wells[3,4] and quantum dots,[5–7] the dark-bright exciton splitting is usually smaller than the thermal energy even at helium temperature. This results in equal population of all band-edge exciton levels and a decrease of the total radiative recombination rate of these semiconductors and semiconductor structures by the ratio of the number of bright emitting exciton states to the total number of the band edge exciton states. This is not the case however for small size colloidal NCs, nanorods and nanoplatelets, where the strong spatial confinement leads to dark-bright exciton splitting on the order dozens of meVs[8–15] and the slow radiative recombination of the dark exciton

affects the photoluminescence (PL) even at room temperature. Although it is practically very important to understand the dark/bright exciton fine structure in all NCs made of all $A_{II}B_{VI}$ and $A_{III}B_{V}$ semiconductors such as CdS, ZnSe, CdTe, or InAs, GaP, InSb, for example, the absolute majority of investigations of the exciton fine structure were conducted only in CdSe NCs. That is why although in this paper we focus on the band edge excitons in the heavily studied CdSe NCs, we are providing general expressions for description of the exciton fine structures in all $A_{II}B_{VI}$ and $A_{III}B_{V}$ semiconductor NCs.

Description of the band edge excitons in CdSe NCs within $1S_{3/2}1S_e$ 8 band model.

The optically passive dark exciton was discovered by Bawendi *et.al.*[16] when the resonance excitation of the PL line of 3.2 nm diameter CdSe NCs showed significant Stokes shift of the PL and μs decay time at helium temperatures. These data were later explained within the Dark/Bright exciton model, which explained also the magnetic field dependence of the PL fine structure observed under resonant excitation.[8,9] The starting point of the model is the assumption of NC spherical symmetry. In spherically symmetric CdSe NC (meaning spherical shaped NCs with a cubic lattice structure or quasi-symmetric NC where the effect of shape asymmetry on the hole energy spectra is compensated by the effect of hexagonal crystal field[9]), the electron ground $1S_e$ level is doubly degenerate with respect to its spin projection, $s_z = \pm 1/2$ and the hole ground $1S_{3/2}$ level is 4-fold degenerate with respect to projections $M = 3/2$, $1/2$, $-1/2$, and $-3/2$ of its total angular momentum, $\boldsymbol{F}$ ($F = 3/2$).[17,18] As a result the absorption band edge and the PL of these NCs is determined by the 8=2x4 optical exciton transitions between these lowest electron and hole levels. The electron-hole exchange interaction:

$$\hat{H}^{exch}_{1S_{3/2}1S_e} = \eta_{1S_{3/2}1S_e}\left[\frac{3}{2}\mathbb{I} - (\boldsymbol{\sigma}_e \cdot \boldsymbol{F})\right] + \overline{\eta}_{1S_{3/2}1S_e}\mathbb{I}, \quad (1)$$

where $\eta_{1S_{3/2}1S_e}$ is the electron-hole exchange constant, $\mathbb{I}$ is the 8x8 unit matrix and $\boldsymbol{\sigma}_e$ is the electron Pauli matrix, splits the 8-fold degenerate exciton state in spherical NCs into the ground optically passive (dark) 5–fold degenerate state with total momentum $\mathcal{F} = 2$ and the upper optically active 3–fold degenerate state with $\mathcal{F} = 1$ by $4\eta_{1S_{3/2}1S_e}$. Equation (1) describes the absolute position of the exciton fine structure levels relative to the reference energy of the lowest optical $1S_{3/2}1S_e$ transition[18] in the absence of exchange, in contrast with Ref. 9, where only the splitting of the exciton fine structure levels were calculated. In addition to the asymmetric splitting of the $\mathcal{F} = 1$ and $\mathcal{F} = 2$ levels described by the first term in Eq.(1), the second term, $\overline{\eta}_{1S_{3/2}1S_e}$, describes an overall shift of all of the fine structure levels from the reference energy. The spherical symmetry can be broken by the

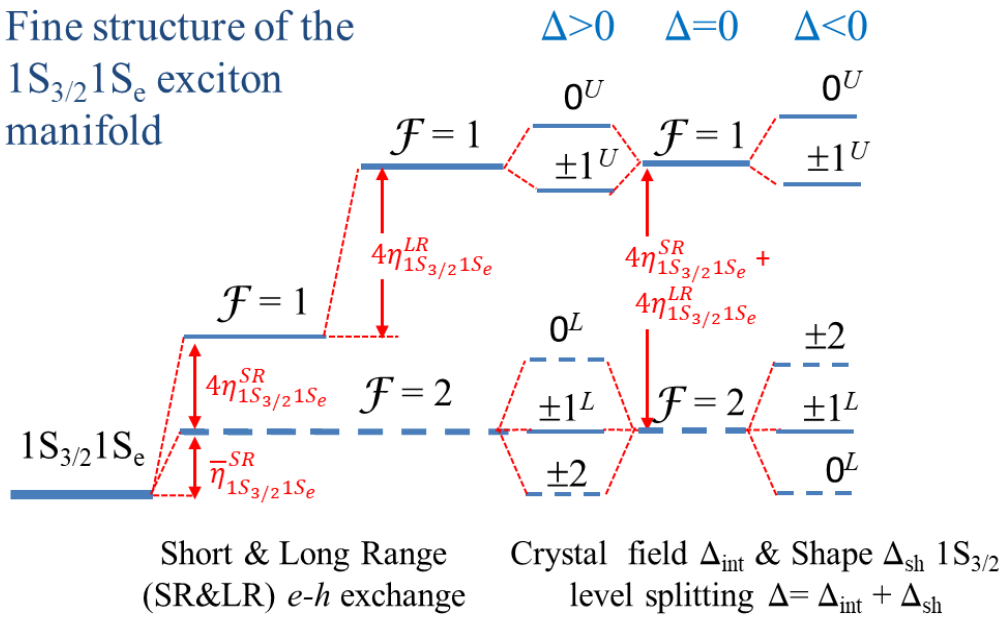

Figure 1: Cartoon showing fine structure of the exciton levels within $1S_e1S_{3/2}$ exciton manifold created by short and long range electron – hole exchange interaction and hole level splitting Δ. The level structure are shown for the case $\Delta > 0$, $\Delta = 0$, and $\Delta < 0$.

internal hexagonal crystal field in semiconductors with wurtzite structure (such as CdSe) and the non-spherical, ellipsoidal shape of NCs. These two effects split $M = \pm 3/2$ and

$M = \pm 1/2$ so called "heavy" and "light" hole sublevels. The splitting is described as[9]

$$\hat{H}^{\rm an} = (\Delta/2)[5/4 - M^2]\,, \tag{2}$$

where the total splitting $\Delta = \Delta_{\rm int} + \Delta_{\rm sh}$ is the sum of the splittings caused by the hexagonal field, $\Delta_{\rm int}$, and by the NC shape, $\Delta_{\rm sh}$.[19] The anisotropy described by Eq. (2) finally results in five band edge exciton states, $\mathcal{F}_z = \pm 2, \pm 1^{L,U}, 0^{L,U}$ with different projections, $\mathcal{F}_z = M + s_z$, on the hexagonal c-axis of the NC. With help of Ref. 9 we can write the absolute position of the exciton fine structure levels as

$$\epsilon_2 = \overline{\eta}_{1S_{3/2}1S_e} - \Delta/2\ ,\ \epsilon_1^{\rm U,L} = \overline{\eta}_{1S_{3/2}1S_e} + 2\eta_{1S_{3/2}1S_e} \pm \sqrt{f^2 + d}\ ,$$
$$\epsilon_0^{\rm U,L} = \overline{\eta}_{1S_{3/2}1S_e} + 2\eta_{1S_{3/2}1S_e} + \Delta/2 \pm 2\eta_{1S_{3/2}1S_e}\ . \tag{3}$$

Here U and L correspond to "+" and "-" signs in the equations for the upper and lower states, respectively, $f = (-2\eta_{1S_{3/2}1S_e} + \Delta)/2$ and $d = 3(\eta_{1S_{3/2}1S_e})^2$. In accordance to Eq. (1) we shift the energy of all levels defined in Ref. 9 to the $1S_e1S_{3/2}$ transition energy by $(3/2)\eta_{1S_{3/2}1S_e} + \overline{\eta}_{1S_{3/2}1S_e}$. The levels are labeled by the projection of the exciton total angular momentum $\mathcal{F}_z$: one level with $\mathcal{F}_z = \pm 2$, two with $\mathcal{F}_z = \pm 1$, and two with $\mathcal{F}_z = 0$. Both of the ± 1 states (lower $1^{\rm L}$ and upper $1^{\rm U}$) are optically active bright excitons. For the states with $\mathcal{F}_z = 0$ only the upper one, $0^{\rm U}$, is optically active, while the lower one, $0^{\rm L}$, is an optically passive dark exciton. The fine structure of the exciton levels within $1S_{3/2}1S_e$ exciton manifold are shown schematically in Fig. 1. One can see that when $\Delta > 0$ (oblate CdSe NCs) the ground exciton is optically forbidden dark exciton with $\mathcal{F}_z = \pm 2$ and when $\Delta < 0$ it is the dark $0^{\rm L}$ exciton level with $\mathcal{F}_z = 0$.[9]

The dark/bright exciton theory developed in Ref. 9 completely neglected the long range exchange interaction. Here it must be made clear that by the terms "long range" and "short range" exchange we are referring in this paper to the non-analytic and analytic portions of the exchange interaction, respectively, as these terms are defined in Refs. 20–22; see note 23.

With this definition, the short-range exchange interaction in the strong confinement regime can be written:[9]

$$\eta^{SR}_{1S_{3/2}1S_e} = \hbar\omega_{ST}\chi_{1S_{3/2}1S_e}(\beta)(a_{ex}/a)^3 \quad (4)$$

where $\hbar\omega_{ST} = 0.13\,\mathrm{meV}$[24] is the short range exchange interaction in bulk CdSe, a_{ex} is the bulk exciton radius, and the dimensionless function $\chi_{1S_{3/2}1S_e}(\beta)$, which depends on the ratio of light- to heavy-hole effective mass, β, is defined in SI via the electron and hole radial wave functions. The short range exchange shift introduced in the SI can be written as $\overline{\eta}^{SR}_{1S_{3/2}1S_e} = \hbar\omega_{ST}\overline{\chi}_{1S_{3/2}1S_e}(\beta)(a_{ex}/a)^3$, where $\overline{\chi}_{1S_{3/2}1S_e}(\beta)$ is also defined in SI via the electron and hole radial wave functions; this term vanishes in the limit $\beta \to 1$ which corresponds to the simple band limit where the $1S_{3/2}$ ground hole level is entirely comprised of $L = 0$ envelope functions. Complete neglect of the long range exchange interaction in Refs. 8,9 was justified by reference to the work of Takagahara,[25] who, using the Wannier function approach, had argued that the long-range exchange interaction vanishes from the exciton fine structure identically in a spherical shape semiconductor NC with simple two-fold degenerate conduction and valence bands. However, this conclusion disagreed with effective mass calculations of the exchange interaction in bound excitons in bulk semiconductors[26] as well as with later calculations of the exchange interaction in semiconductor quantum dots conducted both within the effective mass approximation[27–30] and within the Wannier function approach,[31] collectively indicating that the long range exchange interaction does not vanish in spherical NCs.

An attempt to resolve the controversy was made by Goupalov and Ivchenko who considered the long-range exchange interaction in a bulk semiconductor in the framework of the orthogonal empirical tight-binding model.[32] Goupalov and Ivchenko concluded from this analysis that long range exchange corrections should be included when the band-edge optical transitions are principally inter-atomic (as in the case of anion-to-cation transitions between the nearest neighbors in many binary semiconductors), while in the case that the band-edge optical transitions are principally intra-atomic in nature the long range contribution vanishes in spherical nanocrystals, consistent with the argument of Takagahara.[25] These conclusions,

developed for the simple 2-fold degenerate conduction and valence band case in spherical NC, were generalized to the case of degenerate valence band and it was shown that the analysis based on the effective-mass approximation is valid in case of CdSe NCs, in conjunction with results from pseudopotential calculations.[33] Although the role of the long-range exchange interaction in each semiconductor nano-structure requires generally a special theoretical analysis owing to shape and dielectric confinement effects, the generalization of the Goupalov and Ivchenko results[32] suggests that the long-range exchange interaction is certainly important in semiconductors where the band edge optical transitions occur between two different atoms of the unit cell as is the case of CdSe.

The long-range exchange interaction, $\eta^{LR}_{1S_{3/2}1S_e}$ within the $1S_{3/2}1S_e$ exciton manifold can be written:[27,28,30,31]

$$\eta^{LR}_{1S_{3/2}1S_e} = \frac{\hbar\omega_{LT}}{4}\left(\frac{a_{ex}}{a}\right)^3\left[\xi_{1S_{3/2}1S_e}(\beta) + \left(\frac{\kappa-1}{\kappa+2}\right)\frac{2|Q_0^{(1)}(\beta)|^2}{3}\right] , \qquad (5)$$

where $\hbar\omega_{LT}$ is the bulk exciton longitudinal transverse splitting, which in CdSe is equal to 0.95 meV.[34] The dimensionless functions $\xi_{1S_{3/2}1S_e}(\beta)$ and $Q_0^{(1)}(\beta)$ in Eq. (5) are defined in SI via the electron and hole radial wave functions, and $\kappa = \epsilon_{in}/\epsilon_{out}$ is the ratio of internal, ϵ_{in}, to external, ϵ_{out}, high frequency dielectric constants. In Fig.2 we show the dependences of the dimensionless functions $\xi_{1S_{3/2}1S_e}(\beta)$, $Q_0^{(1)}(\beta)$, $\chi_{1S_{3/2}1S_e}(\beta)$and $\overline{\chi}_{1S_{3/2}1S_e}$ on the ratio of light to heavy- hole effective mass β. The total exchange constant in Eq. (1) is the sum of short- and long- range exchange constants: $\eta_{1S_{3/2}1S_e} = \eta^{SR}_{1S_{3/2}1S_e} + \eta^{LR}_{1S_{3/2}1S_e}$. The long-range term is approximately three time larger than the short-range term in CdSe. Note that the long range exchange, unlike the short range, does not contribute to the overall shift term $\overline{\eta}_{1S_{3/2}1S_e}$.

The fine structure of the exciton levels defined in Eq. (3) depends strongly on the size and shape of the NC. In Fig. 3 we show the size dependence of the exciton fine structure calculated with and without long-range exchange interaction. The optically active and optically

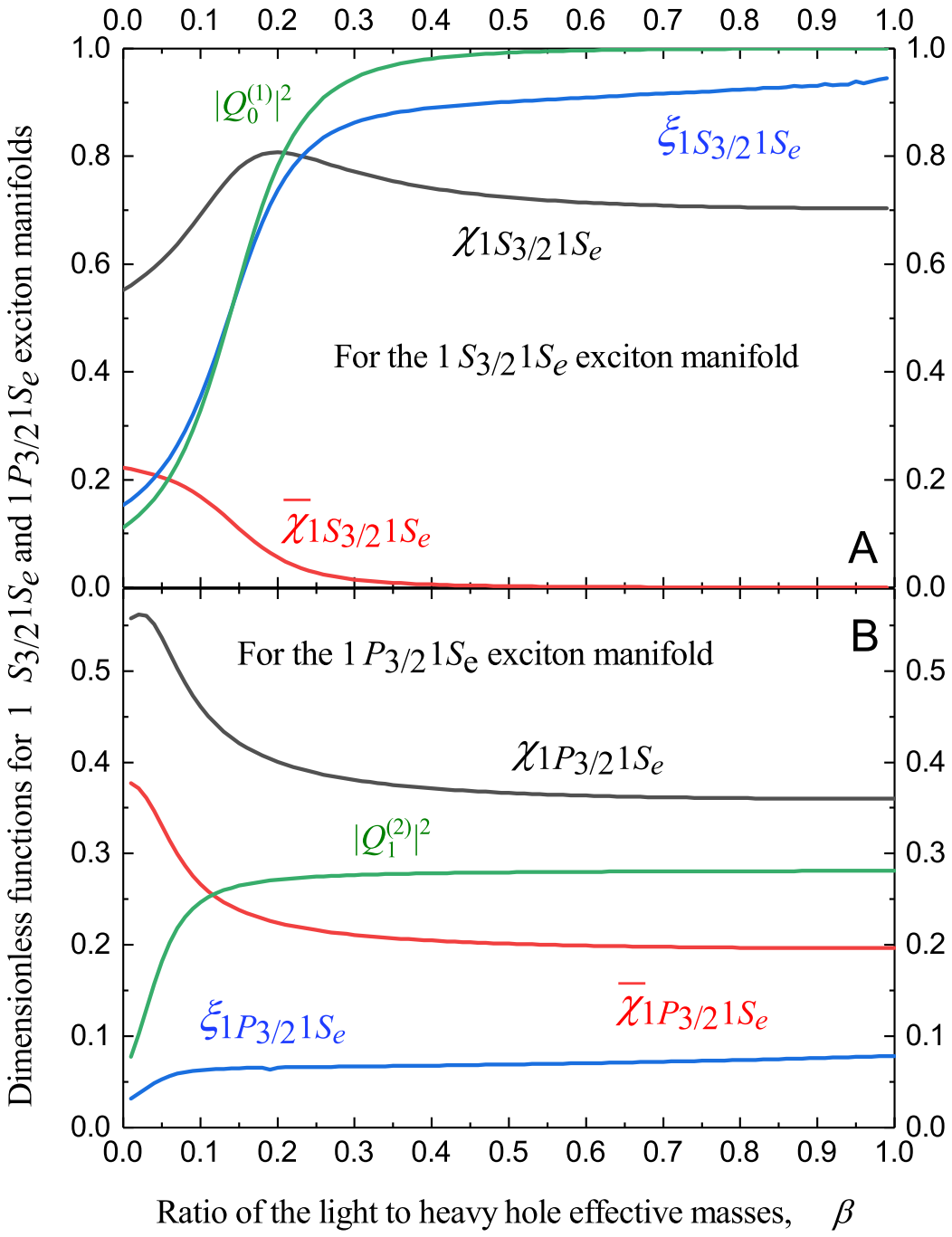

Figure 2: Dependence of dimensionless functions controlling the exciton fine structure on the ratio light to heavy hole effective mass β calculated in SI for (A) - $1S_{3/2}1S_e$ and (B) - $1P_{3/2}1S_e$ exciton manifold.

passive states are shown as solid and dashed lines respectively. One can see that including the long range exchange interaction practically does not affect the distance between the ground ± 2 dark and the first optically active $\pm 1^L$ exciton. Indeed, as is shown in Ref. 9,

this splitting is equal to $3\Delta/4$ in small size NCs where $\eta_{1S_{3/2}1S_e} \gg \Delta$ and it does not depend on $\eta_{1S_{3/2}1S_e}$ in this limit. This explains why the theory, which does not take into account long-range exchange interaction, has described quite well the temperature dependence of PL observed in fluorescence line narrowing experiments.[8,9,35–37] The temperature activation of the resonance PL requires only knowledge of the two lowest exciton levels within the 5 level fine structure.[8,9,38]

At the same time, Fig. 3 B demonstrates that the upper optically active exciton levels 0^U and $\pm1^U$ shift significantly to higher energy if the long-range exchange interaction is taken into account. Consequently the position of these levels, which could be potentially seen in resonant photoluminescence excitation (PLE) experiments, has never been properly described within the theory which neglects the long-range exchange interaction.[39] It was previously demonstrated that the long-range exchange interaction is critical for description of these upper optically active levels.[27,28] In Fig. 3 B we show that even neglecting the deviation of the NC shape from spherical the full theory very well describes the PL Stokes shift and PLE experiments conducted by several experimental groups.

The long range exchange interaction affects also the oscillator transition of the optically allowed transitions. The relative transition strengths of the optically allowed transitions $\pm1^U$, $\pm1^L$ and 0^U can be calculated using Eq. 28 from Ref. 9 simply by replacing $\eta^{SR}_{1S_{3/2}1S_e}$ by the total value $\eta_{1S_{3/2}1S_e} = \eta^{LR}_{1S_{3/2}1S_e} + \eta^{SR}_{1S_{3/2}1S_e}$; the selection rules and polarization properties of the optical transitions remain the same as derived in Ref. 9. The experimental size dependence of the relative oscillator transition strength of the sum of the $\pm1^U$ and 0^U exciton lines and the energetically lower $\pm1^L$ exciton line are shown in Fig.3 C.[39] In the same panel we show the result of the calculations with and without the long range exchange interaction, taking into account the size variation of the nanocrystal ellipticity (see note 30 in Ref. 9) with its concommitant effect on the splitting parameter Δ_{sh}.[19] One can see that the model including long-range exchange clearly describes the experimental data and represents a much better quantitative match than the original model of Ref. 9, where long-range exchange was

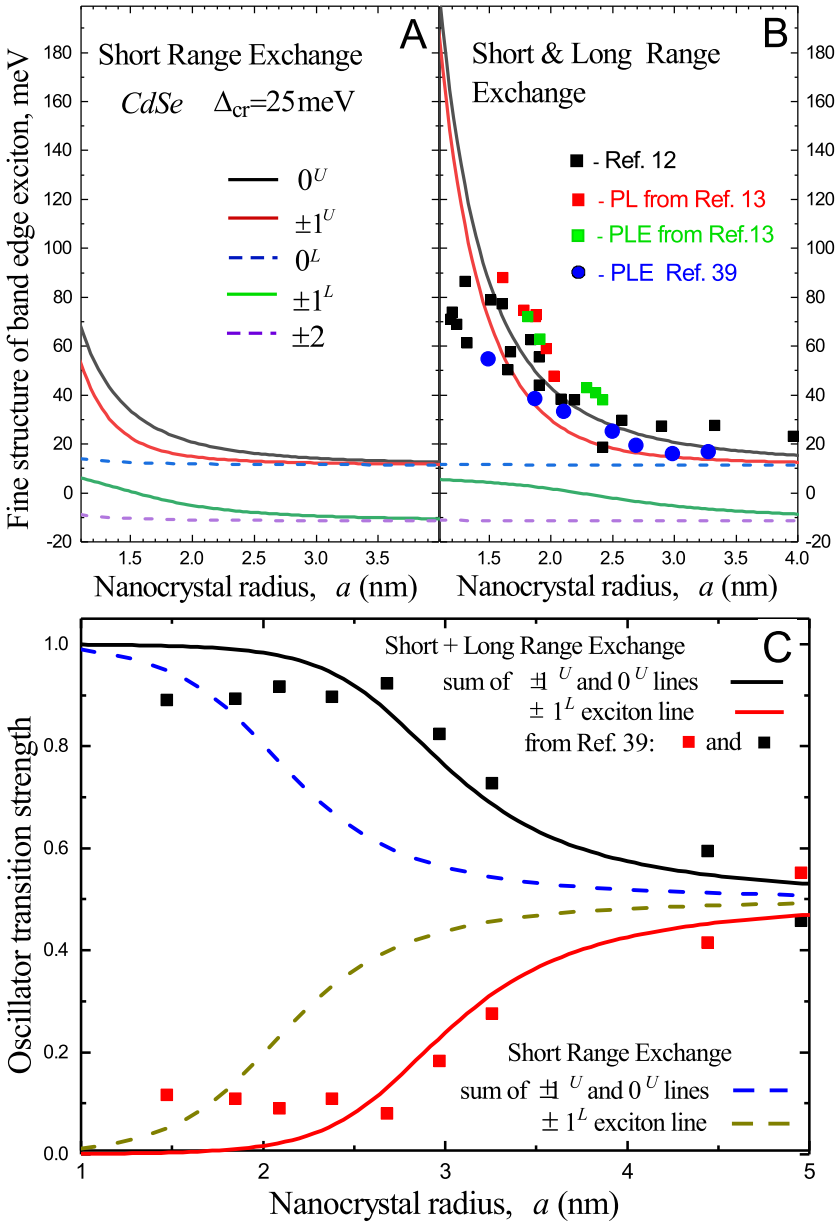

Figure 3: The size dependence of the exciton fine structure calculated for spherical CdSe NCs without (A) and with (B) with long-range exchange interaction. Experimental data showing the position of the the upper optically active level extracted from PL Stokes shift [9,10] and photoluminescence excitation (PLE) experiments. [10,39] In Panel (C), the oscillator transition strength calculated with and without the long range exchange interaction is compared with measured results from Ref. 39 taking into account the size variation of the nanocrystal ellipticity (see note 30 in Ref. 9) with its concomitant effect on the splitting parameter Δ_{sh}. [19]

neglected. More detailed analysis of the effect of the exchange interaction and Δ on the oscillator transition strength is given in the SI.

Band edge excitons in $A_{II}B_{VI}$ and $A_{III}B_{V}$ semiconductor spherical nanocrystals.

In the previous section we have described the fine structure of the band edge exciton in CdSe NCs in the case when only the ground $1S_{3/2}$ hole level participates in the optical transitions. In small size CdSe NCs the ground $1S_{3/2}$ hole level, however, is not very far away energetically from the first excited $1P_{3/2}$ level[18] so that the splitting of these levels caused by the crystal-field, NC shape anisotropy, and the electron-hole exchange interaction can lead to energetic overlap between the $1S_{3/2}1S_e$ and $1P_{3/2}1S_e$ exciton manifolds.

The effect becomes even more pronounced in NCs comprised of semiconductors with spin-orbit coupling, $\Delta_{\rm SO}$, smaller than that of CdSe, where $\Delta_{\rm SO}$ is 420 meV. The effect of $\Delta_{\rm SO}$ on the order of the spacing between hole levels can be analyzed within the 6-band model.[40,41] Indeed, calculations within the 6-band model demonstrated that the $1S_{3/2}$ and $1P_{3/2}$ hole levels can switch order with decrease of the NC size resulting in the $1P_{3/2}$ state becoming the ground hole confinement level, lying below the $1S_{3/2}$ hole levels in small size CdS NC,[40] with $\Delta_{\rm SO} = 62$ meV, and in InP NC, with $\Delta_{\rm SO} = 108$ meV.[41]

The order and the relative energy of the $1S_{3/2}1S_e$ and $1P_{3/2}1S_e$ exciton transitions is also affected by the Coulomb interaction between electron and hole. Taking into account the image charge connected with discontinuity of the dielectric constants at the NC surface and the self-interaction of the electron and hole with their own images, this interaction can be written as:

$$U(\boldsymbol{r}_e, \boldsymbol{r}_h) = -\frac{e^2}{\epsilon_{in}|\boldsymbol{r}_e - \boldsymbol{r}_h|} - V_{im}(\boldsymbol{r}_e, \boldsymbol{r}_h) + \frac{1}{2}V_{im}(\boldsymbol{r}_e, \boldsymbol{r}_e) + \frac{1}{2}V_{im}(\boldsymbol{r}_h, \boldsymbol{r}_h) \ . \qquad (6)$$

The image charge correction $V_{im}(\boldsymbol{r}_e, \boldsymbol{r}_e)$ in Eq.(6) for spherical shape NC can be written

using the Kirkwood expansion:[43]

$$V_{im}(\boldsymbol{r}_e, \boldsymbol{r}_h) = \frac{4\pi e^2}{(2l+1)} \frac{\kappa - 1}{\epsilon_{in} a} \sum_{l,m} \frac{(l+1)}{[l\kappa + (l+1)]} \left(\frac{r_e r_h}{a^2}\right)^l Y_l^{m*}(\theta_e, \phi_e) Y_l^m(\theta_h, \phi_h) \ , \qquad (7)$$

where $Y_l^m(\theta, \phi)$ are the spherical harmonics defined as in Ref. 44. Averaging out Eq.(6) over the wave functions of the $1S_{3/2}1S_e$ and $1P_{3/2}1S_e$ excitons, we find that the Coulomb correction to the independent particle transition energy, can be written as:

$$\Delta E_{ex}^c = -\frac{e^2}{\epsilon_{in} a} \left[f_{ex}(\beta) - \zeta_{ex}(\beta, \kappa) \right] \ . \qquad (8)$$

The first term in Eq.(8) proportional to $f_{ex}(\beta)$ is the result of the averaging of the direct Coulomb interaction between the electron and hole described by the first term in Eq. (6). In the case of simple parabolic bands, when the transition occurs between $1S_e$ and $1S_h$ confined levels $f_{1S_h 1S_e} \approx 1.8$.[45] The second term in Eq.(8) proportional to $\zeta_{ex}(\beta, \kappa)$ is the result of averaging the carrier interactions with mirror charges described by the last three terms in Eq. (6). This interaction vanishes when $\kappa = 1$ as one can see from Eq. (7). The dependences $f_{ex} - \zeta_{ex}$ on β calculated for the $1S_{3/2}1S_e$ and $1P_{3/2}1S_e$ exciton manifolds for several κ are shown in Fig. 4a. One can see that all these Coulomb corrections decrease as κ increases and for $\beta > 0.1$ resulting in a larger red-shift of the transition energy in the $1S_{3/2}1S_e$ exciton manifold than in the $1P_{3/2}1S_e$ one.

Fine structure of the $1P_{3/2}1S_e$ exciton manifold

The fine structure of the $1P_{3/2}1S_e$ exciton manifold is similar to the fine stricture structure of the $1S_{3/2}1S_e$ exciton manifold. It also consists of 5 sub-levels, $\mathcal{F}_z = \pm 2, \pm 1^{L,U}, 0^{L,U}$ characterized by the different projections, $\mathcal{F}_z = M + s_z$, on the hexagonal c-axis of the NC. We will start consideration of this level structure with calculations of the effect of the electron hole exchange interaction. As shown in the SI the interaction can be written as a

sum of short- and long-range exchange terms:[30]

$$\tilde{H}^{ex}_{1P_{3/2}1S_e} = \eta^{SR}_{1P_{3/2}1S_e}\left\{\frac{3}{2}\mathbb{I} - (\boldsymbol{\sigma}_e \cdot \boldsymbol{F})\right\} + \overline{\eta}^{SR}_{1P_{3/2}1S_e}\mathbb{I} + \eta^{LR}_{1P_{3/2}1S_e}\left\{(\boldsymbol{\sigma}_e \cdot \boldsymbol{F}) + \frac{5}{2}\mathbb{I}\right\} \qquad (9)$$

with short-range exchange constants,

$$\eta^{SR}_{1P_{3/2}1S_e} = \hbar\omega_{ST}\chi_{1P_{3/2}1S_e}(\beta)\left(\frac{a_{ex}}{a}\right)^3,\ \overline{\eta}^{SR}_{1P_{3/2}1S_e} = \hbar\omega_{ST}\overline{\chi}_{1P_{3/2}1S_e}(\beta)\left(\frac{a_{ex}}{a}\right)^3, \qquad (10)$$

and a long-range exchange constant,

$$\eta^{LR}_{1P_{3/2}1S_e} = \frac{\hbar\omega_{LT}}{4}\left(\frac{a_{ex}}{a}\right)^3\left[\xi_{1P_{3/2}1S_e}(\beta) + \left(\frac{\kappa-1}{2\kappa+3}\right)\frac{|Q^{(2)}_1(\beta)|^2}{5}\right]. \qquad (11)$$

The dimensionless functions $\chi_{1P_{3/2}1S_e}(\beta)$, $\overline{\chi}_{1P_{3/2}1S_e}(\beta)$, $\xi_{1P_{3/2}1S_e}(\beta)$ and $Q^{(2)}_1(\beta)$ in Eq. (10) and (11) are defined in SI via the electron and hole radial wave functions. Figure 2B shows the dependences of these functions on β. Note that as within the $1S_{3/2}1S_e$ manifold, there is an overall shift of the $1P_{3/2}1S_e$ exciton levels due to short range exchange, which can be written as $\overline{\eta}^{SR}_{1P_{3/2}1S_e}$.

Equation (9) shows the qualitatively different roles played by the long range and short range exchange interactions within the $1P_{3/2}1S_e$ exciton manifold. As was first shown by Ajiki and Cho,[30] the long range exchange correction for the excited $1P_{3/2}1S_e$ states is proportional to $\sim[(\boldsymbol{\sigma}_e \cdot \boldsymbol{F}) + (5/2)\mathbb{I}]$ and therefore shifts the $\mathcal{F} = 2$ levels upwards while leaving the $\mathcal{F} = 1$ levels unshifted. This is in the contrast to the shift pattern produced by the short range exchange, which shifts the $\mathcal{F} = 1$ levels. It is also notable that the $1P_{3/2}1S_e$ states show a non-zero long range exchange correction, despite the fact that these states are dipole forbidden due to parity; this point runs counter to the common intuition that only dipole-active states can show a long range exchange and was handled incorrectly by the current authors in Ref. 46. Since the long range exchange effect in NCs is due to longitudinal electric feild coupling, it should not be expected that the selection rules would be the same

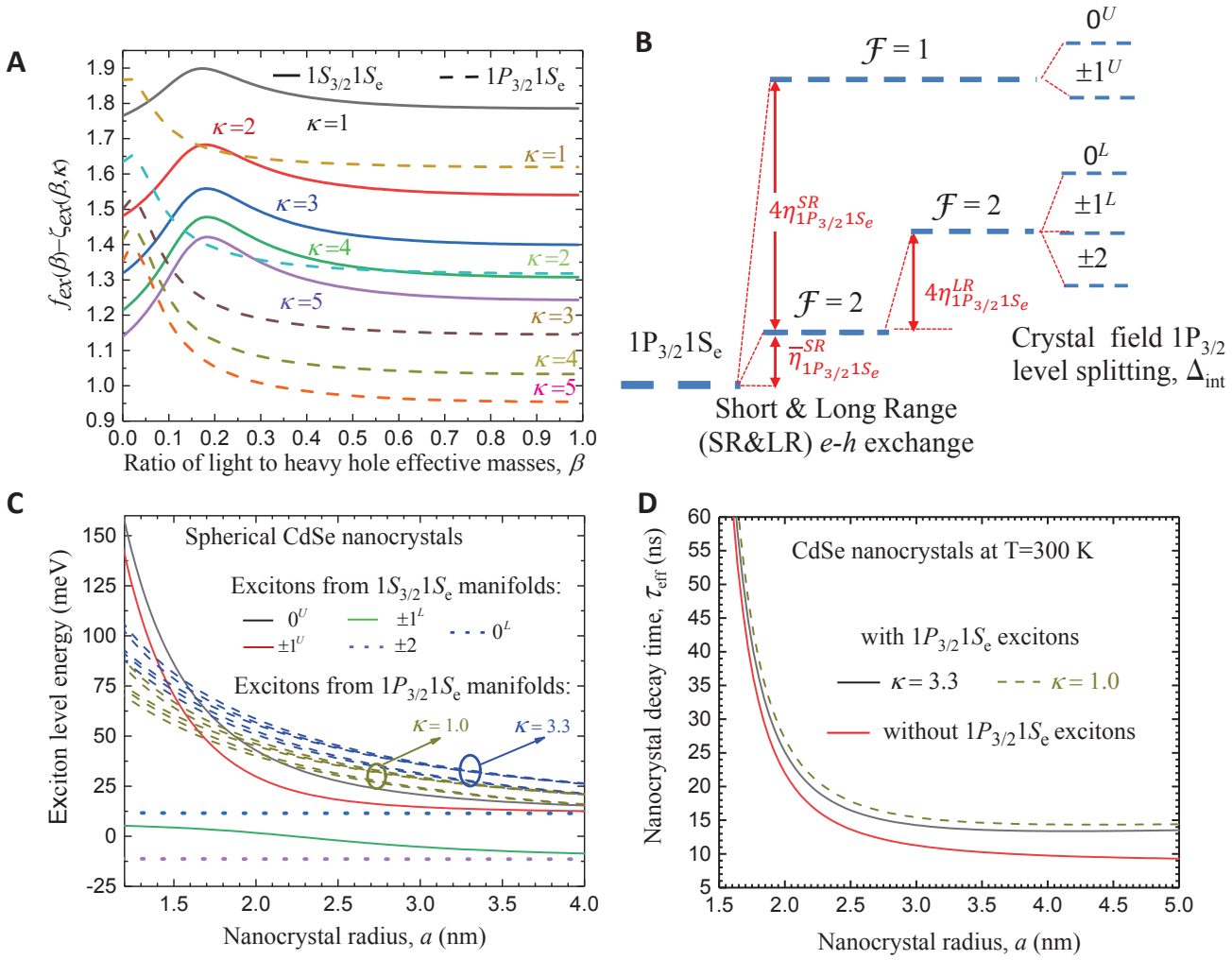

Figure 4: Effect of the $1P_{3/2}1S_e$ exciton manifold on the optical properties of CdSe nanocrystals. A- Dependence of Coulomb corrections to the optical transition energy on the ratio of light- to heavy-hole effective mass, β, calculated for five values of the ratio of the dielectric constant of the semiconductor to the surrounding media, κ. B- fine structure of the $1P_{3/2}1S_e$ exciton manifold, created by the long and short range exchange interaction and crystal field splitting. C- size dependence of the band edge exciton level structure. D- size dependence of the room temperature decay time with and without the $1P_{3/2}1S_e$ exciton manifold. To demonstrate the effect of Coulomb corrections of the optical transition energy on the decay time (panels C and D) these corrections were also calculated using $\kappa = 1$, see text.

as for coupling to propagating transverse electric fields.

The $1P_{3/2}$ hole levels are also split by the internal hexagonal crystal field in semiconductors with wurtzite structure and the non-spherical, ellipsoidal shape of NCs. The fine structure of the exciton levels for the $1P_{3/2}1S_e$ exciton manifold are shown qualitatively in

the cartoon in Fig. 4B. The splitting is described quantitatively by Eq. (2), with a splitting magnitude $\Delta_{1P_{3/2}}$ that is different from the splitting of $1S_{3/2}$ hole levels Δ.[46] For the rest of this paper we will consider only spherical shaped NC where the splitting is due to the intrinsic hexagonal lattice structure. In this case the splitting Δ_{int} of the $1S_{3/2}$ and $1P_{3/2}$ hole level is proportional the bulk crystal field splitting Δ_{cr} and can be written as $\Delta_{1S_{3/2}} = \Delta_{cr} v_{1S_{3/2}}(\beta)$ and $\Delta_{1P_{3/2}} = \Delta_{cr} v_{1P_{3/2}}(\beta)$ respectively, where the dimensionless functions $v_{1S_{3/2}}(\beta)$ and $v_{1P_{3/2}}(\beta)$ are defined in Refs. 9 and 46, respectively.

The resulting energy of the exciton levels from the $1S_e 1P_{3/2}$ exciton manifold can be written in the following form:

$$\begin{aligned}
\epsilon_{2;1P_{3/2}1S_e} &= \overline{\eta}^{SR}_{1P_{3/2}1S_e} + 4\eta^{LR}_{1P_{3/2}1S_e} - \Delta_{1P_{3/2}}/2 \ , \\
\epsilon^{\pm}_{1;1P_{3/2}1S_e} &= \overline{\eta}^{SR}_{1P_{3/2}1S_e} + 2(\eta^{SR}_{1P_{3/2}1S_e} + \eta^{LR}_{1P_{3/2}1S_e}) \pm \sqrt{(f_{1P_{3/2}1S_e})^2 + d_{1P_{3/2}1S_e}} \ , \\
\epsilon^{\pm}_{0;1P_{3/2}1S_e} &= \overline{\eta}^{SR}_{1P_{3/2}1S_e} + 2(\eta^{SR}_{1P_{3/2}1S_e} + \eta^{LR}_{1P_{3/2}1S_e}) + \Delta_{1P_{3/2}}/2 \pm 2\eta_{1P_{3/2}1S_e} \ , \qquad (12)
\end{aligned}$$

where $\eta_{1P_{3/2}1S_e} = \eta^{SR}_{1P_{3/2}1S_e} - \eta^{LR}_{1P_{3/2}1S_e}$, $f_{1P_{3/2}1S_e} = (\Delta_{1P_{3/2}} - 2\eta_{1P_{3/2}1S_e})/2$ and $d_{1P_{3/2}1S_e} = 3(\eta_{1P_{3/2}1S_e})^2$. The size-dependent fine structure of the $1P_{3/2}1S_e$ and $1S_{3/2}1S_e$ exciton manifolds calculated for spherical CdSe NCs is shown in Fig. 4C. In this plot, the quantum size level energy difference between the $1P_{3/2}1S_e$ and $1S_{3/2}1S_e$ excitons in the absence of fine structure splitting was calculated using the 6-band model[18] while the Coulomb correction, Eq.8, is calculated using the 4-band wave functions. Use of the 4-band versus the 6-band wave functions greatly simplifies the expressions while causing only a small error of $\sim$ 12meV at the smallest radius calculated, $a = 1.2$nm; on the other hand, use of the 4-band quantum size level energies would create an unacceptably large error of $\sim$ 57 meV at this radius. States with optically allowed and forbidden transitions are shown by solid and dashed lines, respectively. One can see that optically passive excitons from the $1P_{3/2}1S_e$ manifold overlap energetically with the $1S_{3/2}1S_e$ exciton manifold.

Effect of $1P_{3/2}1S_e$ exciton manifold on the nanocrystal photoluminescence

Optical selection rules do not allow transitions between the $1P_{3/2}$ hole and the $1S_e$ electron levels in $A_{II}B_{VI}$ and $A_{III}B_V$ semiconductor spherical nanocrystals, due to the different parity of the wave functions of these states and, consequently, all eight $1P_{3/2}S_e$ exciton states are dipole forbidden. This generally increases the total number of optically passive dark excitons at the band edge from 5 to 13 and decreases the radiative decay rate by a factor 3/16 at high temperatures for which the exciton states from both the $1P_{3/2}1S_e$ and the $1S_{3/2}1S_e$ manifolds are equally populated. The characteristic radiative decay rate $1/\tau_{ex}$ in $A_{II}B_{VI}$ and $A_{III}B_V$ semiconductor spherical nanocrystals, is described as:

$$\frac{1}{\tau_{ex}} = \frac{8\omega n E_p}{9 \cdot 137 m_0 c^2} \mathcal{D}^2 K \ , \tag{13}$$

where ω is the frequency of emitting light, n is the refractive index of the media, E_p is the Kane energy parameter, m_0 is the fee electron mass, $\mathcal{D} = 3\varepsilon_{\text{out}}/(2\varepsilon_{\text{out}} + \varepsilon_{\text{in}})$ is the depolarization factor, $\varepsilon_{\text{out}} = n^2$ and ε_{in} are high frequency dielectric constants of the media and semiconductor, respectively, and $K = |\int d^3r_e d^3r_h \Psi_{ex}(\boldsymbol{r}_e, \boldsymbol{r}_h)\delta(\boldsymbol{r}_e - \boldsymbol{r}_h)|^2$ is the square of the overlap integral between the electron and hole within the wave function of a confined exciton $\Psi_{ex}(\boldsymbol{r}_e, \boldsymbol{r}_h)$. The estimation conducted for CdSe NCs in hexane ($n = 1.38$) gave $\tau_{ex} \approx 3.3\,\text{ns}$[46] and consequent calculation with the current model leads to the room temperature (RT) radiative decay time of $\sim 16\,\text{ns}$ in NC with radius $a = 2.5\,\text{nm}$. For temperatures that populate all 16 band edge excitons the decay time can be estimated as $\tau_{rd} = (16/3)\tau_{ex} \approx 17.6\,\text{ns}$. This estimation indicates clearly that at RT some of the upper optically active exciton states from the $1P_{3/2}1S_e$ manifolds are only partially populated.

The Coulomb correction generally increases the distance between $1S_{3/2}1S_e$ and $1P_{3/2}1S_e$ exciton manifolds reducing the effect of $1P_{3/2}1S_e$ exciton levels on the radiative decay time.

Importantly this distance significantly increases with κ as one can see in Fig. 4A. In Fig. 4C we show the the size dependence of the $1P_{3/2}1S_e$ exciton manifold calculated for $n = 1.38$ and $n = \sqrt{\epsilon_{in}}$. We show also the size dependence for the case where Coulomb corrections were calculated using $\kappa = 1$ while leaving the exchange and dielectric depolarization factors unchanged. One can see that in this test case the $1P_{3/2}1S_e$ excitons practically overlap with the $1S_{3/2}1S_e$ exciton manifold, which increases the RT decay time. The dependence of the RT decay time on the nanocrystal radius is shown in Fig. 4D. One can see that introduction of the $1P_{3/2}1S_e$ exciton manifold increases the radiative decay time by a factor of two in large NCs. The calculated RT decay in large NCs ~ 15 ns is comparable to the experimental decay time measured on 2 nm radius CdSe NC.[48]

In the opposite case when only excitons from the $1S_{3/2}1S_e$ exciton manifold contribute to PL and all exciton levels are populated the typical RT decay time can be estimated as $\tau_{rd} = (8/3)\tau_{ex} \approx 8.6$ ns. Indeed, significant shortening of the RT radiative decay time in CdSe based NCs was observed recently.[49] In continuously graded core/multi shell CdSe/$Cd_xZn_{1-x}Se$/$ZnSe_{0.5}S_{0.5}$ NCs the RT exciton decay time was measured to be 11.6 ns. This suggests that in the "parabolic shape" confinement potential created in these NCs, the optically passive $1P_{3/2}S_e$ exciton manifold is shifted to higher energy and remains un-populated at room temperature, resulting in radiative decay time shortening. This lifetime is consistent with our calculation of the effective lifetime in CdSe NCs embedded in glass with $n = 1.5$ which gives 10.8 ns in 3nm radius NCs and 18.6 ns on 2nm radius NC.

In this letter, the band-edge excitons and their radiative decay times were calculated for the simplest NC structures, consisting of a spherical shaped CdSe core embedded in media with a homogeneous dielectric constant ϵ_{out}. The effects of a NC shell and of the organic molecules passivating the NC surface were completely neglected. These phenomena affect the magnitude of the short and long range exchange interaction, modifying the exciton fine structure, and the distance between $1S_{3/2}S_e$ and $1P_{3/2}S_e$ exciton manifold. In addition they modify the magnitude of the exciton coupling with light described by exciton radiative decay

time τ_{ex} defined in Eq.(13). For more complex NC structures, and/or NC structures made of various $A_{II}B_{VI}$ and $A_{III}B_{V}$ semiconductors, however, this Letter provides a road map for realistic calculations of the band edge excitons and their decay time.

At low temperatures, when only the lower levels or just the lowest exciton level is populated, the radiative decay times are usually $\sim \mu$s.[8,9] In the case that the ground dark exciton state belongs to the $1S_e1S_{3/2}$ manifold, multiple external mechanisms, such as phonon- , dangling bond -, and magnetic field - assisted recombination of this state have been discussed.[50] Another intrinsic approach to the PL activation was suggested in Ref. 46. It was shown there that the reduction of the QD symmetry to C_s results to the activation of all dark exciton states. The symmetry reduction can be realized by modification of the QD shape, or by introduction of immobile charges within the NC interior or at the NC surface.[51,52] The breaking of the inversion symmetry is critical for the activation of the dark exciton.[46]

In summary we have outlined the major results which are necessary for the quantitative description of the PL in $A_{II}B_{VI}$ and $A_{III}B_{V}$ semiconductor spherical nanocrystals. The long-range exchange interaction significantly increases the band-edge Stoke's shift and should be taken into account for description of photoluminescence excitation spectra. The long decay time of small size NCs at room temperatures is partially connected with thermal occupation of the optically passive $1P_{3/2}1S_e$ exciton manifold.

Supporting Information Available: Details on electronic structure calculation including: Band edge exciton wave functions and energies; the short- and long- range exchange interaction; Analytical results for the $1S_{3/2}1S_e$ and $1P_{3/2}1S_e$ exciton state manifolds; and more detailed analysis of the effect of the long-range exchange interaction and crsytal field splitting on the oscillator strength.

Acknowledgments. Al.L.E. acknowledges the financial support of the Office of Naval Research (ONR) through the Naval Research Laboratory Basic Research Program.

The authors declare no competing financial interests.

References

(1) Becker, M. A.; Vaxenburg, R.; Nedelcu, G,; Sercel, P. C.; Shabaev, A,; Mehl, M. J.; Michopoulos, J. G.; Lambrakos, S. G.; Bernstein, N.; Lyons, J. L.; Stiferle, T.; Mahrt, R. F.; Kovalenko, M. V.; Norris, D. J.; Raino, G.; Efros, Al. L. *Nature* **2018**, *553*, 189 - 193.

(2) R. S. Knox, *Theory of excitons* Academic Press, New York and London, 1963.

(3) Jeukens, C. R. L. P. N.; Christianen, P. C. M.; Maan, J. C.; Yakovlev, D. R.; Ossau, W.; Kochereshko, V. P.; Wojtowicz, T.; Karczewski, G.; Kossut, *Phys. Rev. B* **2002**, *66*, 235318.

(4) Kusrayev, Yu. G.; Zakharchenya, B. P.; Karczewski, G.; Wojtowicz, T.; Kossut, J. *Solid State Commun.* **1997**, *104*, 465-468.

(5) Bayer, M.; Ortner, G.; Stern, O.; Kuther, A.; Gorbunov, A. A.; Forchel,A.; Hawrylak, P.; Fafard, S.; Hinzer, K.; Reinecke, T. L.; Walck, S. N.; Reithmaier, J. P.; Klopf, F.; Schaäfer, F. *Phys. Rev. B* **2002**, *65*, 195315.

(6) Smoleński, T.; Kazimierczuk, T.; Goryca, M.; Jakubczyk, T.; Kłopotowski, Ł.; Cywiński, Ł.; Wojnar, P.; Golnik, A.; Kossacki, P. *Phys. Rev. B.* **2012** *86*, 241305(R).

(7) Korkusinski M.; Hawrylak, P.; *Phys. Rev. B.* **2013**, *87*, 115310.

(8) Nirmal, M. D.; Norris, J.; Kuno, M.; Bawendi, M. G.; Efros, Al. L.; Rosen, M. *Phys. Rev. Lett.* **1995**, *75*, 3728-3731.

(9) Efros, Al. L.; Rosen, M.; Kuno, M.; Nirmal, M.; Norris, D. J; & Bawendi, M. G. *Phys. Rev B* **1996**, *54*, 4843-4856.

(10) Chamarro, M.; Gourdon, C.; Lavallard, P.; Lublinskaya O.; Ekimov, A. I. *Phys. Rev B.* **1996**, *53*, 1336-1342.

(11) Efros, Al. L. *Semiconductor and Metal Nanocrystals: Synthesis and Electronic and Optical Properties* edited by V. I. Klimov, Ch. 3, p. 103 Marcel Dekker, New York, 2003.

(12) Califano, M.; Franceschetti, A; Zunger, A. *Phys. Rev. B* **2007**, *75*, 115401.

(13) Korkusinski, M.; Voznyy, O; Hawrylak, P. *Phys. Rev. B* **2010**, *82*, 245304.

(14) Shabaev A.; Efros, AL. L. *Nano Letters* **2004**, *4*, 1821-1825.

(15) Biadala, L.; Liu, F.; Tessier, M. D.; Yakovlev, D. R.; Dubertret, B.; Bayer, M. *Nano Lett.* **2014**, *14*, 1134-1139.

(16) Bawendi, M. G.; Wilson, W. L.; Rothberg, L.; Carroll, P. J.; Jedju, T. M.; Steigerwald, M. L.; Brus, L. E. *Phys. Rev. Lett.* **1990**, *65*, 1623-1626.

(17) Efros, Al. L.; Rodina, A. V. *Solid State Commun.* **1989**, *72*, 645-648.

(18) Ekimov, A. I.; Hache, F.; Schanne-Klein, M. C.; Ricard, D.; Flytzanis, C.; Kudryavtsev, I. A.; Yazeva, T. V.; Rodina, A.V.; Efros, Al. L. *J. Opt. Soc. Am. B.* **1993**, *10*, 100-107.

(19) Efros, Al. L.;Rodina, A.V. *Phys. Rev. B.* **1993**, *47*, 10005-10007.

(20) Pikus, G.E.; Bir, G.L. *Zh. Eksp. Teor. Fiz.* **1971**, *60*, 195-208. [*Soviet Physics JETP* **1971** *33* 108-114].

(21) Cho, K. *Phys. Rev. B* **1976**, *14*, 4463-4482.

(22) Rossler, U.; Trebin, H.-R. *Phys. Rev. B* **1981**, *23*, 1961-1970.

(23) The separation of the exchange interaction into analytic/ non-analytic portions is closely related, but not identical to, the definitions of short- and long-range exchange as these term are used in analyses based on the Wannier site-function basis.[21,22]

(24) Kochereshko, V. P.; Mikhailov, G. V.; Ural'tsev,I. N. *Fiz. Tverd. Tela* **1983**, *25*, 759-761 [*Sov. Phys. Solid State* **1983**, *25*, 439-442].

(25) Takagahara. T. *Phys. Rev. B.* **1993**, *47*, 4569 -4584.

(26) Pikus, G.E.; Bir, G. L. *Zh. Eksp. Teor. Fiz.* **1972**, *62*, 324-332; [*Soviet Physics JETP* **1972**, *35*, 174-178].

(27) Goupalov, S. V.; Ivchenko. E. L. *J. Cryst. Growth* **1998**, *184/185*, 393 -397; *Acta Physica Polonica* **1998**, *A94*, 341-346.

(28) Goupalov, S. V.; Ivchenko. E. L. *Fiz. Tverd. Tela* **2000**, *42*, 1976 -1984; [*Phys. Sol. Stat.* **2000** *42*, 2030-2038].

(29) Cho, K. *J. Phys. Soc. Jap.* **1999**, *68*, 683-691.

(30) Ajiki H; Cho, K. *International Journal of Modern Physics B.* **2001**, *15*, 3745-3748.

(31) Ajiki H; Cho, K. *Phys. Rev. B.* **2000**, *62*, 7402-7412.

(32) Goupalov, S. V.; Ivchenko. E. L. *Fiz. Tverd. Tela* **2001**, *43*, 1791-1798 . [*Phys. Sol. Stat.* **2001**, *43*, 1867-1875].

(33) Franceschetti, A.; Wang, L. W.; Fu, H.; Zunger, A. *Phys. Rev. B.*, **1998** *58*, 13367-13370 (R).

(34) Kiselev, V. A.; Razbirin, B. S.; Uraltzev, I. N. *Phys. Stat. Sol. (B)* **1975**, *72*, 161-172.

(35) Biadala, L.: Louyer, Y.: Tamarat, Ph.; Lounis, B. *Phys. Rev. Lett.* **2009**, *103*, 037404.

(36) Biadala, L.; Louyer, Y.; Tamarat, Ph.; Lounis, B. *Phys. Rev. Lett.* **2010**, *105*, 157402.

(37) Louyer, Y.; Biadala, L.; Tamarat, Ph.; Lounis, B. *Appl. Phys. Lett.* **2010**, *96*, 203111.

(38) Labeau, O.; Tamarat, Ph.; Lounis, B. *Phys. Rev. Lett.* **2003**, *90*, 257404.

(39) Norris, D.; Efros, Al. L.; Rosen, M.; Bawendi, M. *Phys. Rev. B* **1996**, *53*, 16347-16354.

(40) Grigoryan, G. B.; Kazarayn, E. M.; Efros, Al. L.; Yazeva, T. V. *Sov. Phys. Solid State* **1990**, *32*, 1031-1035.

(41) Richard, T.; Lefebvre, P.; Mathieu, H.; Alle'gre, J. *Phys. Rev. B.* **1996**, *53*, 7287- 7298.

(42) Efros Al. L.; Rosen M. *Phys. Rev B.* **1998**, *58*, 7120 - 7135.

(43) Kirkwood, J. G. *J. Chem. Phys.* **1934**, *2*, 351-361.

(44) Edmonds, A. R. *Angular momentum in Quantum mechanics*, Princenton University Press, 1957.

(45) Brus, L. E. *J. Chem Phys.* **1984**, *80*, 4403-4409.

(46) Sercel, P. C.; Shabaev, A.; Efros, Al. L. *Nano Lett.* **2017** *17*, 4820-4830.

(47) Sercel P. C.; Vahala, K. J. *Phys. Rev. B.* **1990**, *42,* 3690 -3710.

(48) Crooker, S. A.; Barrick, T.; Hollingsworth, J. A.; and Klimov, V. I. *Appl. Phys. Lett.* **2003**, *82*, 2793–2795.

(49) Lim, J.; Park, Y.-S.; Klimov, V. I. *Nature Material* **2018**, *17*, 42-49.

(50) Rodina, A. V.; Efros, Al. L. *Phys. Rev. B.* **2016**, *93*, 155427.

(51) Efros, Al. L.; Nesbitt, D. J.*Nature Nanotechnology* **2016**, *11*, 661-671.

(52) Sercel, P. C.; Shabaev, A.; Efros, Al. L.*MRS Advances* **2018**, *3,* 711-716.